OPEN

# Altered whole-brain gray matter volume in high myopia patients: a voxel-based morphometry study

Xin Huang[a,*], Yuxiang Hu[a,*], Fuqing Zhou[b], Xiaoxuan Xu[a], Yifan Wu[d], Rongpu Jay[d], Yi Cheng[a], Jun Wang[c] and Xiaorong Wu[a]

**High myopia (HM) was associated with impaired long-distance vision. Previous neuroimaging studies showed that abnormal visual experience leads to dysfunction in brain activity in HM even corrected. However, whether alterations in brain structure occur in HM remains unknown. In this study, we analyzed the difference in the whole-brain gray matter volume (GMV) and white matter volume between HM patients and healthy controls (HCs) using a voxel-based morphology method. A total of 82 HM patients (52 men and 30 women) and 58 HCs (28 men and 30 women), matched closely in terms of age and education, were enrolled in this study. All participants underwent MRI scans. The MRI data were processed using the SPM8 software. The relationship between the mean GMV values of the brain regions and clinical features, including refractive diopter and the mean retinal nerve fiber layer thickness, in the HM group were analyzed using Pearson's correlation. Compared with HCs, HM patients showed significantly decreased GMV values in the right cuneus/lingual gyrus and the right thalamus. In contrast, HM groups showed higher GMV values in the brain stem, right parahippocampal gyrus/thalamus, left parahippocampal gyrus/thalamus, as well as the right and the left putamen. No significantly different white matter volume values were found between the two groups. Moreover, in the HM group, the mean retinal nerve fiber layer of the left eye showed a negative correlation with the mean GMV values of the brain stem ($r = -0.218$; $P = 0.049$), right parahippocampal gyrus/thalamus ($r = -0.262$; $P = 0.017$), left parahippocampal gyrus/thalamus ($r = -0.249$; $P = 0.024$), and left putamen ($r = -0.232$; $P = 0.036$). We found that HM patients showed an altered brain structure in the visual pathway regions and the limbic system, which may provide useful information to explore the neural mechanisms of impaired long-distance vision in HM.**


**NeuroReport** 2018, **29**:760–767

**Keywords: gray matter volume, high myopia, magnetic resonance imaging, voxel-based morphometry, white matter volume**

Departments of [a]Ophthalmology, [b]Radiology, Jiangxi Province Medical Imaging Research Institute, The First Affiliated Hospital of Nanchang University, [c]Second Department of Respiratory Disease, Jiangxi Provincial People's Hospital, Nanchang and [d]The Class 2 of Clinical Medicine, Grade 2013, Xiangnan University, Chenzhou, People's Republic of China

Correspondence to Xiaorong Wu, PhD, Department of Ophthalmology, The First Affiliated Hospital of Nanchang University, Nanchang 330006, People's Republic of China
Tel: +86 136 1709 3259; fax: +86 791 8869 2520; e-mail: wxr98021@126.com

*Xin Huang and Yuxiang Hu contributed equally to the writing of this article.

**Received** 5 March 2018 **accepted** 19 March 2018

## Introduction

High myopia (HM) is a common eye disease characterized by impaired long-distance vision. Myopia has become a public health problem globally. According to a survey in China, the prevalence of myopia is about 80% in 18-year-old school children [1]. Furthermore, the prevalence of HM among young Asian adults is 6.8–21.6% [2]. HM is not only a refractive error problem but also associated with severe ocular complications such as retinal detachment [3], macular holes [4], and primary open-angle glaucoma [5]. Currently, excimer laser refractive surgery [6] and intraocular lens surgery [7] are the main HM treatments.

Changes in the ocular shape are the most important pathological changes in HM patients as they affect the diopter. Previously, it has been shown that the eye dimensions of myopia patients are enlarged compared with the emmetropia group [8]. Furthermore, Moriyama *et al.* [9] showed that pathologic myopia patients have an abnormal ocular shape and that this is correlated with vision-threatening conditions. In addition, HM can lead to deformation of the sclera, which is closely related to fundus lesions [10]. Optical coherence tomography (OCT) is an effective and noninvasive method to gain insight into myopic fundus lesions. Using spectral-domain OCT, Sergin *et al.* [11] found that HM patients show lower retinal nerve fiber layer (RNFL) thicknesses than low myopia patients. Furthermore, high myopic eyes show a thinning of the choroidal layer, as has been shown by spectral-domain OCT [12]. Mo *et al.* [13] reported that pathologic myopia is accompanied by a decrease in the macular vascular flow densities. The above-mentioned studies mainly focused on pathological ocular changes in HM patients. However, little is known about whether visual systems, including the visual pathways, are altered in HM.

Functional MRI has been used to assess altered brain activity in HM patients as myopia after corneal refractive



0959-4965 Copyright © 2018 The Author(s). Published by Wolters Kluwer Health, Inc. DOI: 10.1097/WNR.0000000000001028

surgery would affect the activation in the visual cortex [14,15]. Nelles *et al.* [16] showed an increased activation in the oculomotor and visual networks of refractive error patients. Furthermore, Zhai *et al.* [17] reported that HM patients have a decreased long-range functional connectivity density in the inferior temporal gyrus, the supramarginal gyrus, and the rostrolateral prefrontal cortex. In our previous study, we found that HM patients showed low-frequency fluctuations with an abnormal amplitude in many brain regions related to language understanding and attentional control [18]. However, the above-mentioned studies focused on the alterations in brain function activities. Whether abnormal visual experience would lead to the plasticity of brain structure in HM remains unknown.

The brain structure is related to risk factors and functional outcomes. Aging or neurological disorders may cause changes in neuroanatomy. Voxel-based morphometry (VBM) is an automated method for analyzing neuromorphological MRI data and is applied widely to evaluate changes in the gray and white matter volume (GMV and WMV, respectively) in the brain [19]. In recent years, the VBM method has been applied successfully to investigate brain morphological changes in many diseases such as optic neuritis [20], Alzheimer's disease [21], and Parkinson's disease [22].

Here, we determine whether the HM patients showed alterations in GMV and WMV relative to healthy controls (HCs) (emmetropia). Furthermore, the relationships between the mean GMV and WMV values of brain regions and clinical features in HM patients were analyzed using Pearson's correlation. We hypothesized that abnormal visual experience in adult HM patients would lead to cross-modal plasticity in brain structure.

## Participants and methods

### Participants

In total, 82 HM patients (52 men and 30 women) were enrolled from the Ophthalmology Department of the First Affiliated Hospital of Nanchang University. The diagnostic criteria of HM were as follows: (i) refractive diopter less than –6.00; (ii) absence of any other ocular diseases (strabismus, amblyopia, cataracts, glaucoma, retinal degeneration, etc.). The exclusion criteria were as follows: (i) HM with myopia-related complications (retinal detachment, cataracts, and myopic maculopathy); (ii) history of ocular trauma or eye surgery; (iii) cardiovascular system diseases, such as heart disease and hypertension; and (iv) psychiatric disorders and cerebral infarction diseases.

Fifty-eight HCs (28 men and 30 women) were also recruited for this study. The inclusion criteria were as follows: (i) absence of any ocular disease with uncorrected visual acuity (VA) greater than 1.0; (ii) absence of cardiovascular system diseases (heart disease, hypertension, etc.); (iii) absence of psychiatric disorders (depression, bipolar disorder, etc.); and (iv) eligibility for MRI scanning (i.e. absence of cardiac pacemaker or implanted metal devices).

The research protocol followed the Declaration of Helsinki and was approved by the Medical Ethics Committee of the First Affiliated Hospital of Nanchang University. All participants provided an informed consent form.

### Ophthalmic testing

In HM groups, the mean retinal nerve fiber layer (RNFL) thicknesses of both eyes were calculated for each patient using CIRRUS HD-OCT (version 3.0, Carl Zeiss Meditec, Inc., Dublin, California, USA). The log MAR values of the best-corrected VA of both eyes were measured in the HM group, and the refractive diopter and the mean keratometric readings were calculated using an autorefractometer (ARK-700A; Nidek, Gamagori, Japan).

### Image acquisition

MRI scanning was performed on a 3-T MRI scanner (Siemens, Erlangen, Germany) with an eight-channel head coil. High-resolution T1-weighted images were acquired using a three-dimensional spoiled gradient-recalled sequence with the following parameters: repetition time = 1900 ms, echo time = 2.26 ms, thickness = 1.0 mm, gap = 0.5 mm, acquisition matrix = 256 × 256, field of view = 250 × 250 mm, flip angle = 9°, and slices = 176.

### Magnetic resonance imaging data preprocessing

All MRI data were preprocessed using VBM following the diffeomorphic anatomical registration through the exponentiated lie algebra (DARTEL) approach [23] using the Statistical Parametric Mapping software (SPM8; *http://www.fil.ion.ucl.ac.uk/spm*) implemented in MATLAB 2013a (MathWorks, Natick, Massachusetts, USA). Preprocessing included the following steps: (i) all structural images were checked by an experienced radiologist to eliminate unqualified participants because of head motion and image artifacts; (ii) all MRI data were aligned with the anterior and posterior commissure lines on the transverse plane; (iii) structural images were segmented into gray matter (GM), white matter (WM), and cerebrospinal fluid areas on the basis of the International Consortium of Brain Mapping template using the unified standard segmentation option in SPM8. After segmentation, the individual WM and GM components were normalized into the standard Montreal Neurological Institute (MNI) template with a voxel size of $1.5 \times 1.5 \times 1.5\,mm^3$ and modulated for GM and WM volumes using the DARTEL approach. Finally, the resulting GMV and WMV images were smoothed with an 8-mm full-width at half-maximum Gaussian kernel.

### Statistical analysis

All data are indicated as mean ± SD. A one-sample *t*-test [$P < 0.05$, false discovery rate (FDR) corrected] was performed to extract the GM and WM volumes across

Table 1 Demographics and clinical measurements by group

| Conditions | HM (mean ± SD) | HC (mean ± SD) |
|---|---|---|
| Male/female | 52/30 | 28/30 |
| Age (years) | 23.29 ± 1.36 | 22.42 ± 1.47 |
| Weight (kg) | 68.15 ± 5.95 | 67.63 ± 5.28 |
| Handedness | 82R | 58R |
| Duration of HM (years) | 8.38 ± 1.23 | NA |
| Refractive diopter-right (D) | −658.97 ± 33.55 | NA |
| Refractive diopter-left (D) | −658.29 ± 32.94 | NA |
| Best-corrected VA-right eye | 1.12 ± 0.11 | 1.17 ± 0.16 |
| Best-corrected VA-left eye | 1.15 ± 0.13 | 1.16 ± 0.15 |
| Mean retinal nerve fiber layer OD (μm) | 263.53 ± 21.80 | NA |
| Mean retinal nerve fiber layer OS (μm) | 266.74 ± 18.46 | NA |

HC, healthy control; NA, not applicable; OD, oculus dexter; OS, oculus sinister; VA, visual acuity.

the participants within the HM group as well as the HCs. Then, second-level general linear models and a two-sample *t*-test were performed to compare the GMV and WMV values between the two groups using SPM8 with age and sex as nuisance covariates, a threshold of $P$ less than 0.05, and a cluster FDR for the multiple comparison correction. To exclude global nuisance effects, total intracranial volumes of each participant were also entered into the design matrix as a global calculation. The MNI coordinates of the GMV and WMV were analyzed using the MRIcron software (*http://www.mricro.com*) [24]. We did not find significantly different WMV values between the two groups ($P > 0.05$).

The mean GMV values in the different brain regions of the two groups were analyzed using the receiver operating characteristic (ROC) curve method. Furthermore, Pearson's correlation was used to evaluate the relationship between the mean GMV values in different brain regions in the HM group and behavioral performances using SPSS, version 16.0 (SPSS Inc., Chicago, Illinois, USA). Differences with values of $P$ less than 0.05 were considered statistically significant.

## Results

### Demographics and visual measurements

HM patients as well as HCs showed an age range of 23.29 ± 1.36 and 22.42 ± 1.47 years, respectively. For the HM group, the mean HM duration was 8.38 ± 1.23 years. Furthermore, the refractive diopters of the right and left eye in the HM group were –658.97 ± 33.55 and –658.97 ± 33.55 diopter, respectively. The best-corrected VA values in the right and left eye in the HM group were 1.12 ± 0.11 and 1.15 ± 0.13 diopter, respectively. The mean RNFL of the oculus dexter and oculus sinister in the HM group were 263.53 ± 21.80 and 266.74 ± 18.46 μm, respectively. More details are shown in Table 1.

### Gray matter volume differences

Intragroup comparison within the HM and HC groups was performed (Fig. 1). Compared with HCs, HM patients showed significantly decreased GMV values in the right cuneus/lingual gyrus and right thalamus [Fig. 2 (black) and Table 2]. In contrast, HM patients showed significantly increased GMV values in the brain stem, right parahippocampal gyrus/thalamus, left parahippocampal gyrus/thalamus, as well as the right and left putamen [Fig. 2 (gray) and Table 2]. Furthermore, altered GMV changes are illustrated in a three-dimensional picture (Fig. 3; cluster > 20 voxels, $P < 0.01$, FDR corrected). The mean values of altered GMVs between the two groups are shown in a histogram (Fig. 4). We did not find any significant differences in the WMV values between the two groups ($P > 0.01$).

### Receiver operating characteristic curve

We speculated that the GMV difference between the two groups might be a useful diagnostic marker. Thus, the mean GMV values in the different brain regions were analyzed using the ROC curve method. The area under the ROC curve in the right cuneus/lingual gyrus was 0.713 [95% confidence interval (CI): 0.624–0.802]; the area under the ROC curve in the right thalamus was 0.800 (95% CI: 0.728–0.872; HM < HCs; Fig. 5a). The area under the ROC curve was 0.835 (95% CI: 0.771–0.899) in the brain stem, 0.782 (95% CI: 0.708–0.856) in the right parahippocampal gyrus/thalamus, 0.782 (95% CI: 0.708–0.855) in the left parahippocampal gyrus/thalamus, 0.739 (95% CI: 0.659–0.819) in the right putamen, and 0.734 (95% CI: 0.652–0.815; HM > HCs; Fig. 5b) in the left putamen.

### Correlation analysis

In the HM group, the left mean RNFL was correlated negatively with the mean GMV signal value of the brain stem ($r = –0.218$; $P = 0.049$; Fig. 6a), right parahippocampal gyrus/thalamus ($r = –0.262$; $P = 0.017$; Fig. 6b), left parahippocampal gyrus/thalamus ($r = –0.249$; $P = 0.024$; Fig. 6c), and left putamen ($r = –0.232$; $P = 0.036$; Fig. 6d) ($P < 0.05$).

## Discussion

To the best of our knowledge, our study is the first to explore changes in the GMV in HM patients and their clinical features. Compared with HCs, HM patients showed significantly decreased GMV values in the right cuneus/lingual gyrus and the right thalamus. Furthermore, HM patients showed higher GMV values in the brain stem, right parahippocampal gyrus/thalamus, left parahippocampal gyrus/thalamus, as well as the right and left putamen. Moreover, in the HM group, the mean RNFL of the left eye was correlated negatively with the mean GMV signal value of the brain stem ($r = –0.218$; $P = 0.049$), right parahippocampal gyrus/thalamus ($r = –0.262$; $P = 0.017$), left parahippocampal gyrus/thalamus ($r = –0.249$; $P = 0.024$), and left putamen ($r = –0.232$; $P = 0.036$).

### Analysis of the gray matter volume decrease of the high myopia group

The cuneus (BA17) is a part of the occipital lobe, which plays an important role in visual processing [25]. The

**Fig. 1**

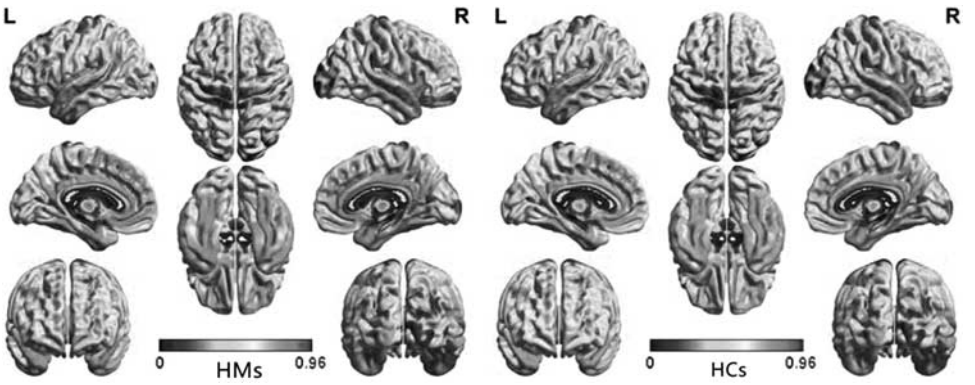


Results of the one-sample *t*-test. Within-group GMV maps in the HM (left) and HC (right) groups ($P < 0.01$, FDR corrected). FDR, false discovery rate; GMV, gray matter volume; HC, healthy control; HM, high myopia; L, left; R, right.

**Fig. 2**

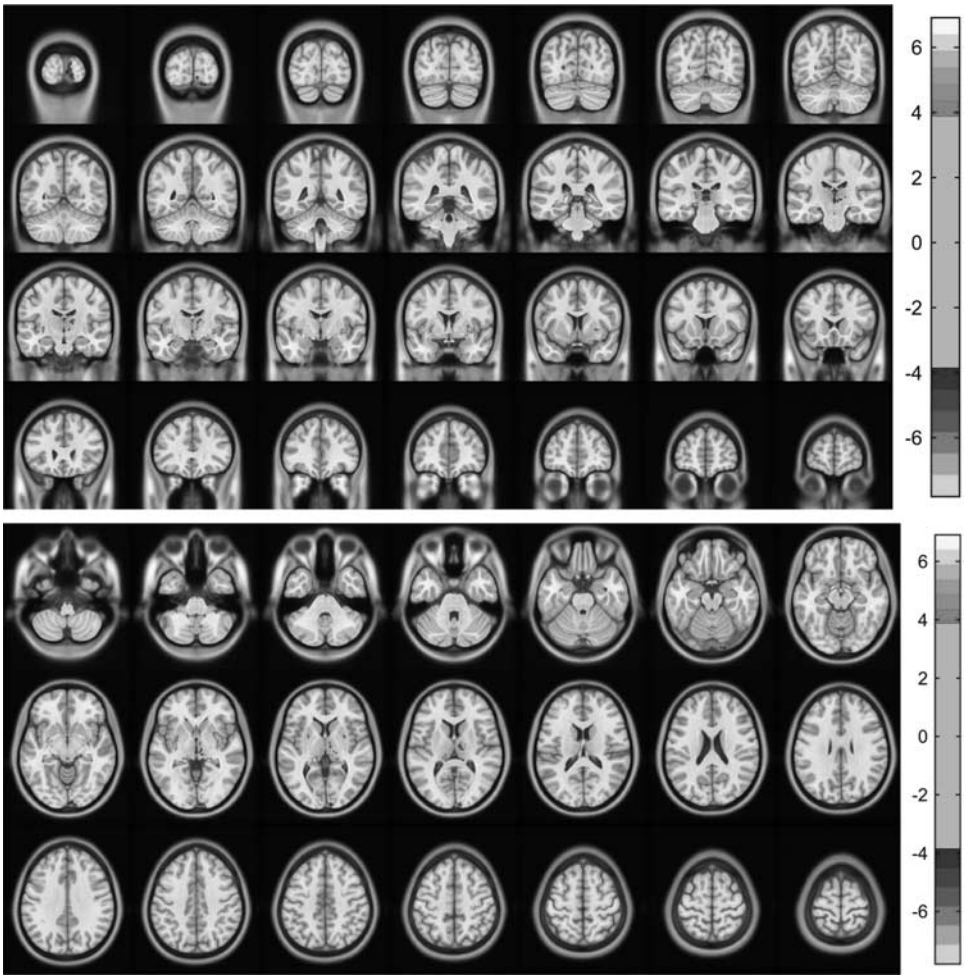


GMV alterations in HM and HC groups. Significant differences in GMV were observed in the right cuneus/lingual gyrus, right thalamus, brain stem, right parahippocampal gyrus/thalamus, left parahippocampal gyrus/thalamus, as well as the right and left putamen. Gray areas denote higher GMV values and black areas indicate lower GMV values ($P < 0.01$ for multiple comparisons using GRF theory; cluster > 20 voxels, $P < 0.01$, FDR corrected). FDR, false discovery rate; GMV, gray matter volume; GRF, Gaussian random field; HCs, healthy controls; HM, high myopia.

**Table 2 Brain areas with significantly different GMV values between two groups**

| Brain areas | BA | Peak MNI coordinate | | | Cluster voxels (1.5 $mm^3$/voxel) | Peak intensity (*t* values) |
|---|---|---|---|---|---|---|
| | | *x* | *y* | *z* | | |
| HM < HC | | | | | | |
| Right cuneus/lingual gyrus | 17.18 | 10.5 | −102 | −1.5 | 345 | −5.940 |
| Right thalamus | – | 15 | −12 | 13.5 | 257 | −7.810 |
| HM > HC | | | | | | |
| Brain stem | – | 9 | −19.5 | −40.5 | 385 | 6.913 |
| Right parahippocampa gyrus/thalamus | 27 | 13.5 | −28.5 | −15 | 266 | 6.597 |
| Left parahippocampa gyrus/thalamus | 27 | −18 | −34.5 | 1.5 | 529 | 6.856 |
| Right putamen | – | 31.5 | 0 | −1.5 | 471 | 5.932 |
| Left putamen | – | −33 | −13.5 | −1.5 | 282 | 5.705 |

The statistical threshold was set at the voxel level with $P < 0.05$ for multiple comparisons using Gaussian random field theory (cluster > 20 voxels, $P < 0.01$, FDR corrected).
BA, Brodmann area; FDR, false discovery rate; GMV, gray matter volume; HCs, healthy controls; HM, high myopia; MNI, Montreal Neurological Institute.

**Fig. 3**

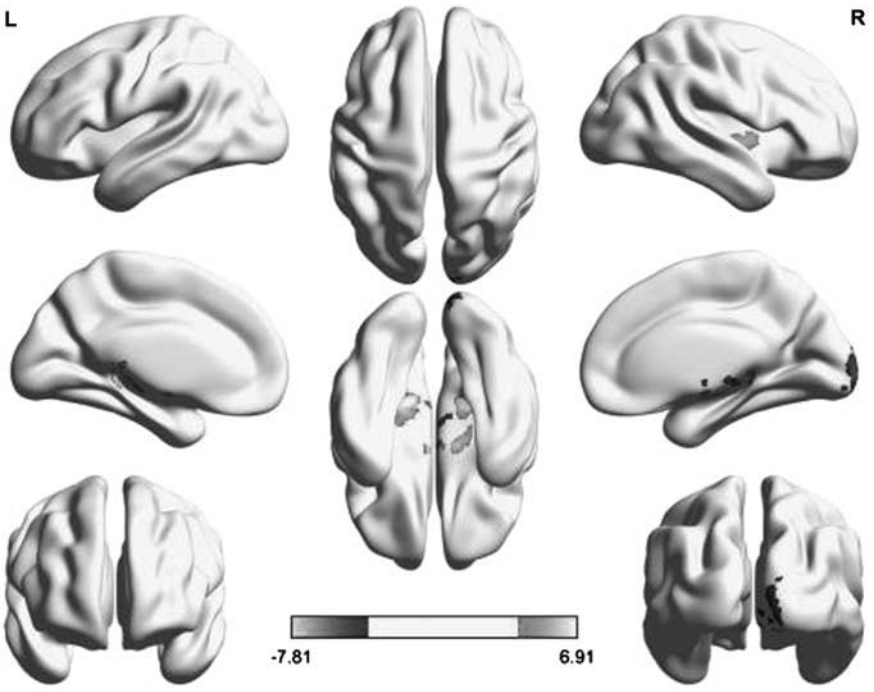


GMV alterations in HM and HC groups with a three-dimensional picture. Significant differences in the GMV were observed in the right cuneus/lingual gyrus, right thalamus, brain stem, right parahippocampal gyrus/thalamus, left parahippocampal gyrus/thalamus, as well as the right and left putamen. Black areas denote higher GMV values and black areas indicate lower GMV values ($P < 0.01$ for multiple comparisons using GRF theory; cluster > 20 voxels, $P < 0.01$, FDR corrected). FDR, false discovery rate; GMV, gray matter volume; GRF, Gaussian random field; HCs, healthy controls; HM, high myopia; L, left; R, right.

anteromedial cuneus interacts with the primary visual cortex (V1) to encode visual information for the extrastriate cortices [26]. Meanwhile, the cuneus is a part of the V1. Mirzajani *et al.* [27] reported that lens-induced myopia decreases the occipital visual cortex activation. Furthermore, the refractive errors had a negative effect on visually evoked magnetic fields in V1 [28]. Our results support these findings and found that HM patients show a marked GMV decrease in the right cuneus gyrus. Therefore, we speculated that HM might be accompanied by impairment in the visual cortex.

The lingual gyrus, known as BA18, is part of the occipital cortex that performs visual processing [29] and is located in the visual cortex 2 (V2), which is an important area in the visual cortex. Furthermore, the lingual gyrus plays a critical role in spatial memory [30] and reading [31]. V2 is a visual association area, which receives strong feedforward connections from V1. Furthermore, V2 is involved in stereo vision [32]. In our study, we found that GMV values of HM patients were decreased in the right lingual gyrus (BA18). We speculated that HM might lead to dysfunction of the brain structure in V2.

The thalamus is located in the forebrain, which plays a critical role in sensory transduction, and is involved in the visual system [33]. The lateral geniculate nucleus is a part of the thalamus [34] that receives signals from the retinal [35] and places the visual information into the visual cortex [36]. Furthermore, the thalamus is involved in cognition [37]. In our study, we showed that HM patients had decreased GMV values in the right thalamus. Furthermore, the area under the ROC curve was 0.800 for the right thalamus. Thus, we speculated that HM might lead to dysfunction of the thalamus.

**Fig. 4**

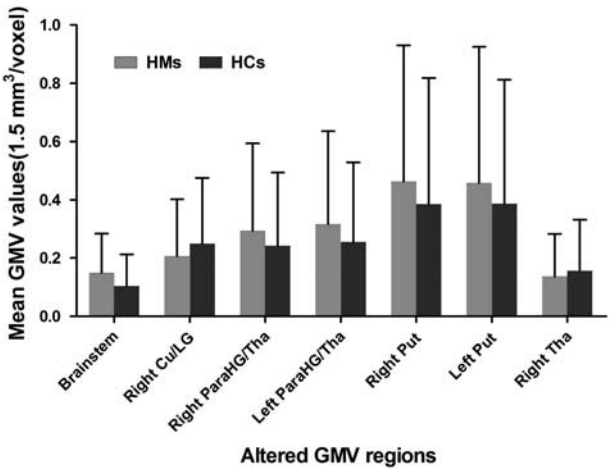


Mean altered GMV values of HM and HC groups. Cu, cuneus; GMV, gray matter volume; HCs, healthy controls; HM, high myopia; LG, lingual gyrus; ParaHG, parahippocampal gyrus; Put, putamen; Tha, thalamus.

### Analysis of the gray matter volume increase in the high myopia group

The parahippocampal gyrus surrounds the hippocampus. The critical role of the parahippocampal gyrus is the memory [38,39], and it is involved in visual memory [40] and environmental encoding [41]. Furthermore, the parahippocampal gyrus and the thalamus are core parts of the limbic system, which plays a critical role in memory and emotions [42]. In our study, we found that HM patients showed increased GMV values in the bilateral parahippocampal gyrus/thalamus and that increased GMV values were correlated negatively with the mean RNFL of the left eye. Thus, we speculated that HM might be associated with dysfunction in memory. Furthermore, brain structural changes in the bilateral parahippocampal gyrus/thalamus might be related to pathological changes in HM.

The putamen is a large nucleus of the basal ganglia, which play a critical role in motor control [43,44], and

**Fig. 5**

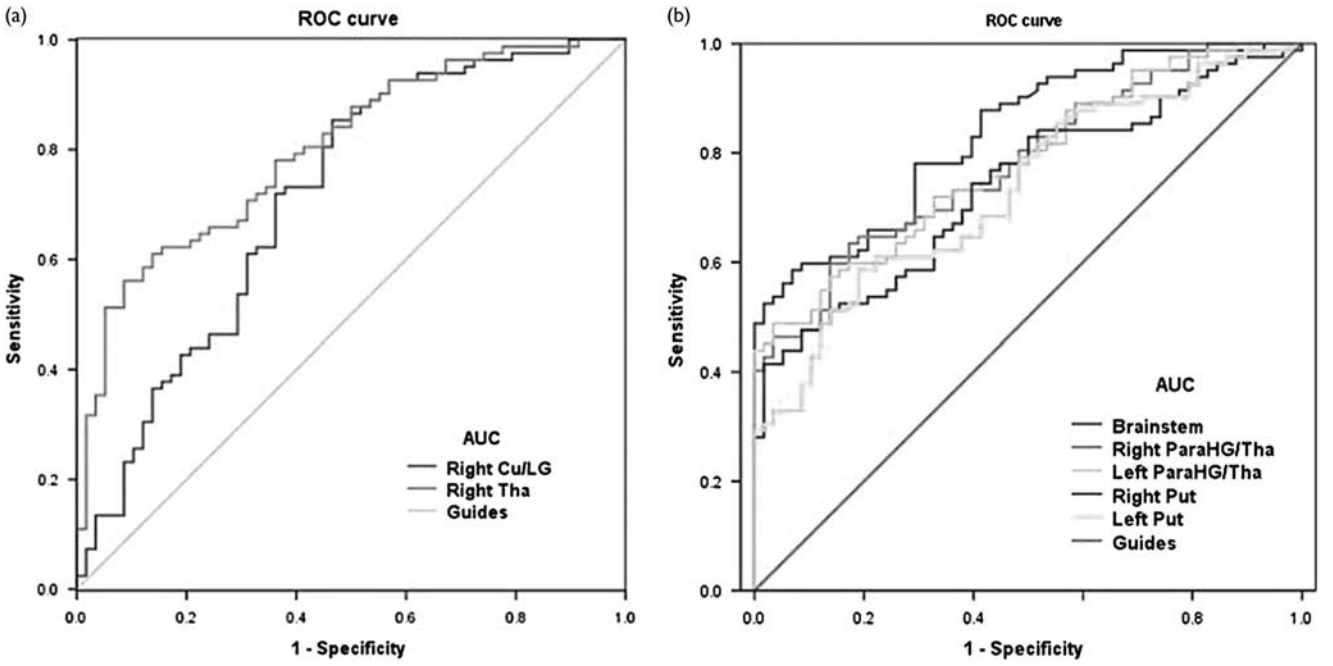


ROC curve analysis of mean GMV values for altered brain regions. (a) The areas under the ROC curve were 0.713 ($P < 0.001$; 95% CI: 0.624–0.802) for the right Cu/LG and 0.800 ($P < 0.001$; 95% CI: 0.728–0.872) for the right Tha (HM < HCs). (b) The areas under the ROC curve were 0.835 ($P < 0.001$; 95% CI: 0.771–0.899) for the brain stem; 0.782 ($P < 0.001$; 95% CI: 0.708–0.856) for the right ParaHG/Tha; 0.782 ($P < 0.001$; 95% CI: 0.708–0.855) for the left ParaHG/Tha; 0.739 ($P < 0.001$; 95% CI: 0.659–0.819) for the right Put; and 0.734 ($P < 0.001$; 95% CI: 0.652–0.815) for the left Put (HM > HCs). AUC, area under the curve; CI, confidence interval; Cu, cuneus; FDR, false discovery rate; GMV, gray matter volume; HCs, healthy controls; HM, high myopia; ROC, receiver operating characteristic; LG, lingual gyrus; ParaHG, parahippocampal gyrus; Put, putamen; Tha, thalamus.

**Fig. 6**

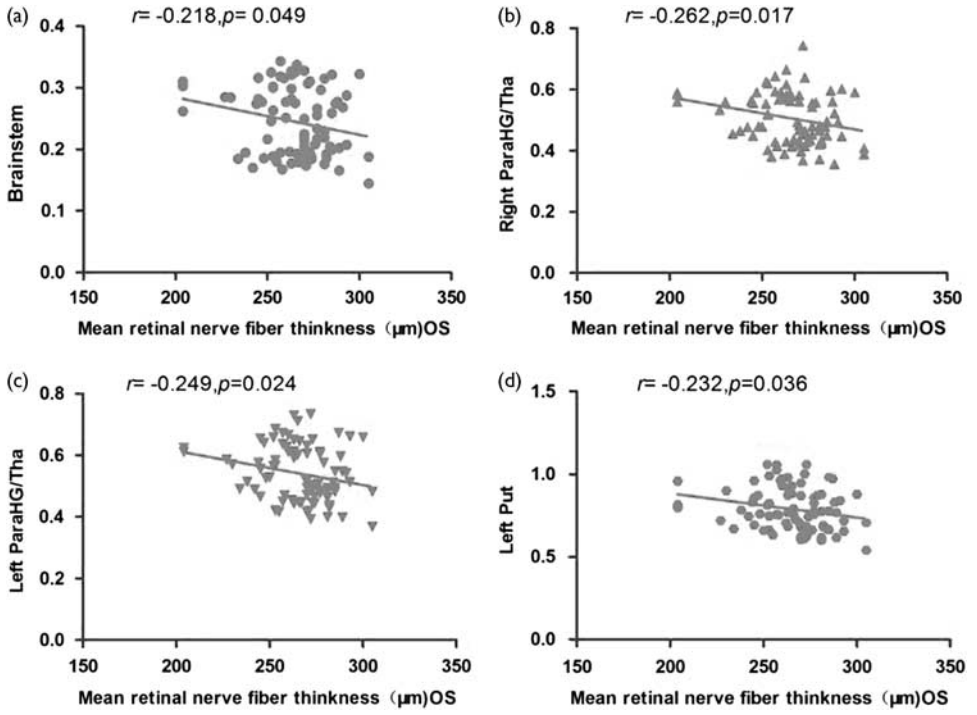


Correlations between the mean GMV signal values of different areas and behavioral performances. The left mean RNFL was correlated negatively with the mean GMV values of (a) the brain stem ($r=-0.218$; $P=0.049$), (b) the right ParaHG/Tha ($r=-0.262$; $P=0.017$), (c) the left ParaHG/Tha ($r=-0.249$; $P=0.024$), and (d) the left Put ($r=-0.232$; $P=0.036$). GMV, gray matter volume; HCs, healthy controls; HM, high myopia; ParaHG, parahippocampal gyrus; OS, oculus sinister; Put, putamen; RNFL, retinal nerve fiber layer thickness; Tha, thalamus.

presents the core part of the basal ganglia network [45]. In addition, the putamen is closely related to learning [46,47]. We found that HM patients showed increased GMV values in the bilateral putamen, which were correlated negatively with the mean RNFL of the left eye. Therefore, we speculated that HM might lead to structural changes of the bilateral putamen, which might reflect the compensation of the motor function in HM. Moreover, the structural changes of the bilateral putamen were correlated with pathological changes in HM.

Our study presents several limitations. First, the HM patients enrolled in this study were mainly young individuals. Second, ophthalmic testing, including OCT, was not performed on the healthy individuals. Third, we could not explain the reason for the increased GMV values in the HM group.

## Conclusion

Our results indicate that HM patients show an abnormal brain structure in visual pathway regions and the limbic system, which might provide some useful information to explain the neural mechanisms in HM.

## Acknowledgements

This study was supported by the National Natural Science Foundation of China (81760179, 81360151); the Natural Science Foundation of Jiangxi Province (20171BAB205046); the Key Foundation of Education Department of Jiangxi Province (GJJ160033); and the Health Development Planning Commission Science Foundation of Jiangxi Province (20185118).

### Conflicts of interest

There are no conflicts of interest.

## References

1 Jonas JB, Xu L, Wei WB, Wang YX, Jiang WJ. Myopia in China: a population-based cross-sectional, histological, and experimental study. *Lancet* 2016; **388**:S20.
2 Wong YL, Saw SM. Epidemiology of pathologic myopia in asia and worldwide. *Asia Pac J Ophthalmol (Phila)* 2016; **5**:394–402.
3 Dragoumis I, Richards A, Alexander P, Poulson A, Snead M. Retinal detachment in severe myopia. *Lancet* 2017; **390**:124.
4 Feng L, Jin X, Li J, Zhai J, Fang W, Mo J, *et al*. Surgical management of retinal detachment resulting from macular hole in a setting of high myopia. *Eye Sci* 2012; **27**:69–75.
5 Ma F, Dai J, Sun X. Progress in understanding the association between high myopia and primary open-angle glaucoma. *Clin Exp Ophthalmol* 2014; **42**:190–197.
6 Barsam A, Allan BD. Excimer laser refractive surgery versus phakic intraocular lenses for the correction of moderate to high myopia. *Cochrane Database Syst Rev* 2014; **6**:D7679.
7 Tian Y, Jiang HB, Jiang J, Wen D, Xia XB, Song WT. Comparison of implantable collamer lens visian ICL V4 and ICL V4c for high myopia: a cohort study. *Medicine (Baltimore)* 2017; **96**:e7294.
8 Pope JM, Verkicharla PK, Sepehrband F, Suheimat M, Schmid KL, Atchison DA. Three-dimensional MRI study of the relationship between eye

dimensions, retinal shape and myopia. *Biomed Opt Express* 2017; **8**:2386–2395.
9 Moriyama M, Ohno-Matsui K, Hayashi K, Shimada N, Yoshida T, Tokoro T, *et al*. Topographic analyses of shape of eyes with pathologic myopia by high-resolution three-dimensional magnetic resonance imaging. *Ophthalmology* 2011; **118**:1626–1637.
10 Ohno-Matsui K, Akiba M, Modegi T, Tomita M, Ishibashi T, Tokoro T, *et al*. Association between shape of sclera and myopic retinochoroidal lesions in patients with pathologic myopia. *Invest Ophthalmol Vis Sci* 2012; **53**:6046–6061.
11 Sezgin AB, Gunay BO, Kardes E, Unlu C, Ergin A. Evaluation of the ganglion cell complex and retinal nerve fiber layer in low, moderate, and high myopia: a study by RTVue spectral domain optical coherence tomography. *Semin Ophthalmol* 2017; **32**:682–688.
12 Gupta P, Thakku SG, Saw SM, Tan M, Lim E, Tan M, *et al*. Characterization of choroidal morphologic and vascular features in young men with high myopia using spectral-domain optical coherence tomography. *Am J Ophthalmol* 2017; **177**:27–33.
13 Mo J, Duan A, Chan S, Wang X, Wei W. Vascular flow density in pathological myopia: an optical coherence tomography angiography study. *BMJ Open* 2017; **7**:e13571.
14 Vuori E, Vanni S, Henriksson L, Tervo TM, Holopainen JM. Refractive surgery in anisometropic adult patients induce plastic changes in primary visual cortex. *Acta Ophthalmol* 2012; **90**:669–676.
15 Malecaze FJ, Boulanouar KA, Demonet JF, Guell JL, Imbert MA. Abnormal activation in the visual cortex after corneal refractive surgery for myopia: demonstration by functional magnetic resonance imaging. *Ophthalmology* 2001; **108**:2213–2218.
16 Nelles G, Pscherer A, de Greiff A, Esser J. Brain activation of eye movements in subjects with refractive error. *Eye Brain* 2010; **2**:57–62.
17 Zhai L, Li Q, Wang T, Dong H, Peng Y, Guo M, *et al*. Altered functional connectivity density in high myopia. *Behav Brain Res* 2016; **303**:85–92.
18 Huang X, Zhou F, Hu Y, Xu X, Zhou X, Zhong Y, *et al*. Altered spontaneous brain activity pattern in patients with high myopia using amplitude of low-frequency fluctuation: a resting-state fMRI study. *Neuropsychiatr Dis Treat* 2016; **12**:2949–2956.
19 Ashburner J, Friston KJ. Voxel-based morphometry: the methods. *Neuroimage* 2000; **11**:805–821.
20 Huang X, Zhang Q, Hu PH, Zhong YL, Zhang Y, Wei R, *et al*. White and gray matter volume changes and correlation with visual evoked potential in patients with optic neuritis: a voxel-based morphometry study. *Med Sci Monit* 2016; **22**:1115–1123.
21 Li X, Wang H, Tian Y, Zhou S, Li X, Wang K, *et al*. Impaired white matter connections of the limbic system networks associated with impaired emotional memory in Alzheimer's disease. *Front Aging Neurosci* 2016; **8**:250.
22 Chen B, Wang S, Sun W, Shang X, Liu H, Liu G, *et al*. Functional and structural changes in gray matter of parkinson's disease patients with mild cognitive impairment. *Eur J Radiol* 2017; **93**:16–23.
23 Ashburner J. A fast diffeomorphic image registration algorithm. *Neuroimage* 2007; **38**:95–113.
24 Kim GW, Jeong GW. White matter volume change and its correlation with symptom severity in patients with schizophrenia: a VBM-DARTEL study. *Neuroreport* 2015; **26**:1095–1100.
25 Plomp G, Leeuwen C, Ioannides AA. Functional specialization and dynamic resource allocation in visual cortex. *Hum Brain Mapp* 2010; **31**:1–13.
26 Vanni S, Tanskanen T, Seppa M, Uutela K, Hari R. Coinciding early activation of the human primary visual cortex and anteromedial cuneus. *Proc Natl Acad Sci USA* 2001; **98**:2776–2780.
27 Mirzajani A, Sarlaki E, Kharazi HH, Tavan M. Effect of lens-induced myopia on visual cortex activity: a functional MR imaging study. *AJNR Am J Neuroradiol* 2011; **32**:1426–1429.
28 Suzuki M, Nagae M, Nagata Y, Kumagai N, Inui K, Kakigi R. Effects of refractive errors on visual evoked magnetic fields. *BMC Ophthalmol* 2015; **15**:162.
29 Bogousslavsky J, Miklossy J, Deruaz JP, Assal G, Regli F. Lingual and fusiform gyri in visual processing: a clinico-pathologic study of superior altitudinal hemianopia. *J Neurol Neurosurg Psychiatry* 1987; **50**:607–614.
30 Sulpizio V, Committeri G, Lambrey S, Berthoz A, Galati G. Selective role of lingual/parahippocampal gyrus and retrosplenial complex in spatial memory across viewpoint changes relative to the environmental reference frame. *Behav Brain Res* 2013; **242**:62–75.
31 Mechelli A, Humphreys GW, Mayall K, Olson A, Price CJ. Differential effects of word length and visual contrast in the fusiform and lingual gyri during reading. *Proc Biol Sci* 2000; **267**:1909–1913.
32 von der Heydt R, Zhou H, Friedman HS. Representation of stereoscopic edges in monkey visual cortex. *Vision Res* 2000; **40**:1955–1967.
33 Usrey WM, Alitto HJ. Visual functions of the thalamus. *Annu Rev Vis Sci* 2015; **1**:351–371.
34 Diao Y, Cui L, Chen Y, Burbridge TJ, Han W, Wirth B, *et al*. Reciprocal connections between cortex and thalamus contribute to retinal axon targeting to dorsal lateral geniculate nucleus. *Cereb Cortex* 2017; **28**:1–15.
35 Williams AL, Reese BE, Jeffery G. Role of retinal afferents in regulating growth and shape of the lateral geniculate nucleus. *J Comp Neurol* 2002; **445**:269–277.
36 Krolak-Salmon P, Henaff MA, Tallon-Baudry C, Yvert B, Guenot M, Vighetto A, *et al*. Human lateral geniculate nucleus and visual cortex respond to screen flicker. *Ann Neurol* 2003; **53**:73–80.
37 Saalmann YB, Kastner S. Gain control in the visual thalamus during perception and cognition. *Curr Opin Neurobiol* 2009; **19**:408–414.
38 Kilpatrick L, Cahill L. Amygdala modulation of parahippocampal and frontal regions during emotionally influenced memory storage. *Neuroimage* 2003; **20**:2091–2099.
39 Yonelinas AP, Hopfinger JB, Buonocore MH, Kroll NE, Baynes K. Hippocampal, parahippocampal and occipital-temporal contributions to associative and item recognition memory: an fMRI study. *Neuroreport* 2001; **12**:359–363.
40 Duzel E, Habib R, Rotte M, Guderian S, Tulving E, Heinze HJ. Human hippocampal and parahippocampal activity during visual associative recognition memory for spatial and nonspatial stimulus configurations. *J Neurosci* 2003; **23**:9439–9444.
41 Pu Y, Cornwell BR, Cheyne D, Johnson BW. The functional role of human right hippocampal/parahippocampal theta rhythm in environmental encoding during virtual spatial navigation. *Hum Brain Mapp* 2017; **38**:1347–1361.
42 Catani M, Dell'Acqua F, Thiebaut DSM. A revised limbic system model for memory, emotion and behaviour. *Neurosci Biobehav Rev* 2013; **37**:1724–1737.
43 Vicente AF, Bermudez MA, Romero MC, Perez R, Gonzalez F. Putamen neurons process both sensory and motor information during a complex task. *Brain Res* 2012; **1466**:70–81.
44 Romero MC, Bermudez MA, Vicente AF, Perez R, Gonzalez F. Activity of neurons in the caudate and putamen during a visuomotor task. *Neuroreport* 2008; **19**:1141–1145.
45 Afifi AK. The basal ganglia: a neural network with more than motor function. *Semin Pediatr Neurol* 2003; **10**:3–10.
46 Brovelli A, Nazarian B, Meunier M, Boussaoud D. Differential roles of caudate nucleus and putamen during instrumental learning. *Neuroimage* 2011; **57**:1580–1590.
47 Grahn JA, Parkinson JA, Owen AM. The role of the basal ganglia in learning and memory: neuropsychological studies. *Behav Brain Res* 2009; **199**:53–60.